Emergent Materials (2022) 5:1517–1531
https://doi.org/10.1007/s42247-021-00338-8

ORIGINAL ARTICLE

Enhanced sequestration of heavy metals from aqueous solution on polyacrylamide grafted with cell@Fe_3O_4 nanocomposite

Rais Ahmad[1] · **Khalid Ansari**[1] · **Mohammad Osama Ejaz**[1]

Received: 30 August 2021 / Accepted: 9 December 2021 / Published online: 31 January 2022

Abstract
Herein, poly(acrylamide)-grafted cell@Fe_3O_4 (PAC@Fe_3O_4) nanocomposite was synthesized through the polymerization process of acrylamide polymers oxidative available radical in the existence of cell@Fe_3O_4 nanomaterial nanoparticles. Various analytical methods including FTIR, SEM, XRD, and TEM were used to characterize the material. The nanocomposite material was studied further for its ability to adsorbed Pb(II), Ni(II), and Cu(II) from wastewater. To optimize adsorption process, the impact of different factors like contact time, temperature, pH, doses, and concentration was performed. Adsorption of metal ion is pH-dependent, with the highest removal efficiency occurring at high pH levels and at pH value 5; the maximum capacities of the chosen metal ions were determined for Pb(II) and Cu(II) while pH 4 for Ni(II). The maximum capacity (q_m) was observed to be 313.02 mg g^{-1} for Pb(II), 219.33 mg g^{-1} for Ni(II), and 210.71 mg g^{-1} for Cu(II), respectively. The kinetic parameters indicate that the metal ion adsorption by PAC@Fe_3O_4 followed second-order kinetics, with chemical adsorption as the rate-limiting step. The nature of adsorption was endothermic and spontaneous demonstrated by positive ΔH° and negative ΔG° values.

Keywords Adsorption · PAC@Fe_3O_4 · Redlich-Peterson · Temkin · TEM · Endothermic

1 Introduction

The global community is currently plaguing with two major crises: energy resources and sustainable development [1, 2]. The discharge of toxic metals in the atmosphere from numerous chemical industries such as mining, refineries, agriculture, and metal plating causes water contamination in humans and ecosystem damage [3–5]. Heavy metal pollution has become a major health concern all over the world due to its inability to decompose and obstinate nature [6]. The most common toxic metals are Pb(II) and Cu(II) found in the water of industry and are found to be highly toxic causing serious illnesses, having a carcinogenic effect, and interfering with the nervous and biological systems in living beings even when the concentration is low [7, 8].

Therefore, much effort has gone into developing environmentally friendly, cost-effective, and efficient heavy metal removal methods, such as ion exchange [9], electro-dialysis [10], chemical precipitation [11], coagulation–flocculation [12], adsorption [13], and membrane filtration [14]. Adsorption has to be the most commonly used method for wastewater remediation because of its excellent adsorption capacity and ease of use with no harmful by-products [15].

Nanocomposites made of biopolymers grafted onto synthetic polymers have recently been investigated for use in a variety of industrial applications, including treating wastewater. Polysaccharides, such as alginate, guar gum, cellulose, pectin, chitosan, and starch, are examples of natural polymers which have inspired scientists' attention in water purification, especially in the areas of heavy metal sequestration because of their physical characteristics, economic viability, and abundance of inclusion complexes of the backbone of the chain [16, 17]. Cellulose, a linear polymer of – 1,4-linked D-glucopyanose monomer, is the utmost profuse biopolymer and it is acts as the main ingredient of paper, membranes, textiles, and among other issues [18]. Due to challenging properties along with renewability, biocompatibility, non-toxicity, and biodegradability, cellulose is a very viable material for synthesizing an adsorbent for heavy metal removal at a low cost [19].

✉ Rais Ahmad
rais45@rediffmail.com

[1] Environmental & Bio-inspired Research Laboratory, Department of Applied Chemistry, Faculty of Engineering & Technology, Aligarh Muslim University, Aligarh 202002, India

Magnetic nanoparticles (MNPs), i.e., Fe_3O_4, are about the most fascinating and technologically significant materials in terms of physical and chemical properties, with a broad spectrum of potential applications [20]. Magnetic nanoparticles based on the phase of solid separation (MNPs–SPE) has proven to be a successful method for removing trace amount of chemical and particulate reagents from biological systems since its introduction [21]. Because of its inherent magnetism, low toxicity, and ease of operation, iron-oxide particles are the most promising adsorbent in MSPE. To remove a variety of pollutants from wastewater, polymer-modified nanoparticles with a high specific surface area and adsorption sites were implemented [22]. Poly(acrylamide) (PAM) is a water-soluble polymer that has a lot of acetyl amino group on its surfactant molecules, it forms hydrogen bonds with aromatic structures, and metal ions can be adsorbed by chemisorption or physiosorption [23–27]. Functionalized materials with well-ordered and tunable porous nanostructures, in particular, have shown great promise for catalysis, adsorption, and molecular separation applications due to their unique properties, such as high porosity and tunable surface chemistry that can be controlled by simple manipulation with organic/inorganic guest species. The main advantage of present material is its high monolayer adsorption capacity as compared to other adsorbents in the literature. The PAC@Fe_3O_4 also exhibits very good regenerative capability, and it can be used up to fourth cycle successfully without much loss in efficiency for the sequestration of Pb(II), Ni(II), and Cu(II) metals.

In present work, PAM chains were grafted onto cell@Fe_3O_4 nanocomposite to enhance the dispersion property as well as adsorption capacity of PAC@Fe_3O_4 in aqueous solution can also be improved to increase the surface functional density. Various analytical methods including SEM, FTIR, XRD, and TEM were used to characterize the material. The nanocomposite material was used to analyze the sequestration of Pb(II), Ni(II), and Cu(II) from wastewater. To optimize the adsorption, the effect of numerous parameters, namely, concentration, temperature, pH, doses, and contact time was performed. The expended adsorbent was desorbed and regenerated in order to make the entire process more cost effective.

2 Materials and methods

2.1 Chemicals

Microcrystalline cellulose and acrylamide were collected from (CDH, New Delhi), liquor ammonia (Fisher Scientific), $FeCl_3.6H_2O$, and $FeCl_2.4H_2O$ (Merck, India), and nitrate salts of respective metal ions were employed as obtained without further purification. Azobisisobutyronitrile (AIBN) was obtained by CDH. Buffer tablets were used exactly as they were attained. The 1000 mg L^{-1} of stock solution was obtained by dissolving requisite amount of metal salts in double-distilled water (DDW).

2.2 Synthesis of cell@Fe_3O_4 nanoparticles

A simplistic process of chemical co-precipitation in a one-step was used to produce the nanoparticles [28]. Briefly, $FeCl_2{\cdot}4H_2O$ (4 g) and $FeCl_3{\cdot}6H_2O$ (8 g) were transferred into 150 mL solution of cellulose (5 g) in DDW of vigorous stirring for 2 h at 1000 rpm. Now, 20 mL of 25% NH_4OH solution was transferred drop wise and the mixture was heat at 90 °C. The solution was kept at 90 °C for 2 h with continuous stirring and a nitrogen atmosphere. The obtained materials were rinsed with DDW to remove impurities and dried at 80 °C.

2.3 Synthesis of poly(acrylamide)-g-cell@Fe_3O_4 nanocomposite

The present PAC@Fe_3O_4 adsorbent was produced by performing in situ polymerization with monomer of acrylamide by free radical in the impendence of cell@Fe_3O_4 nanoparticles [29]. In a round bottom flask with multiple necks, fitted with constant stirring and a reflux condenser, cell@Fe_3O_4 nanoparticles (7.5 g), AIBN (0.05 g), and and acrylamide (5 g) were mixed in 100 mL methanol. For 15 min, the flask was cleansed with dry nitrogen and the solution was allowed to heat up to 60 °C for 6 h while being magnetically stirred. The reaction solution was then relocated to extract with a Soxhelt apparatus for 72 h with a mixture of 50/50 DMF–water. The obtained nanocomposite was then dried for 12 h at 80 °C in an oven.

2.4 Characterization

FTIR spectrum of nanocomposite was found in the frequency range 400 to 4000 cm^{-1} using Perkin-Elmer 1600 model IR spectrophotometer from samples with KBr pallets. The crystalline behavior of cell@Fe_3O_4 nanocomposite was investigated by using X-ray diffractometer (Siemens D 5005) with Cu α radiation ($\lambda = 1.5406$ A°). A SEM (scanning electron microscope) fitted with the use of EDX (energy-dispersive X-ray) spectrometer (model JSM 6510LV, JEOL, Japan) was used to observed the surface morphology and elemental analysis before and after adsorption of present nanocomposite. The particle size of obtained nanocomposite was evaluated with TEM (Transmission Electron Microscope) (JEM 2100, JEOL, Japan). The concentration of metal ions was examined by Atomic Absorption Spectrophotometer (AAS; GBC-902, Australia).

2.5 Adsorption experiments

The adsorption studies were then carried out by using batch equilibrium method in aqueous solutions at pH (1–6), doses (10–50 mg), temperature (30–50 °C), contact time (10–300 min), and concentration (20–100 mg L^{-1}). In a flask, 0.03-g dose of nanocomposite was treated with 20 mL solution of metal ion at the optimal concentration and shaking at 120 rpm in a hot water-bath shaker. After reaching equilibrium, the adsorbent was forced to remove, and the supernatant was obtained. Metal ion concentration in the supernatant was obtained using an AAS flame. Adsorption kinetic studies with 100 mg L^{-1} concentration of metal at optimum pH were carried out over a time range 5–300 min. The influence of metal ion concentration and dose were also examined. The adsorbed amount of adsorbate per unit mass onto PAC@Fe_3O_4 surface was determined by using the following relationship:

$$q_e = \frac{(C_o - C_e)V}{W} \tag{1}$$

where q_e (mg g^{-1}) denotes equilibrium adsorption capacity of nanocomposite; C_o (mg L^{-1}) denotes the initial concentration of metal while C_e (mg L^{-1}) is the concentration after adsorption respectively, V (L) is the volume of the metal ion solution, and W (g) is the adsorbent mass.

2.6 Desorption studies

Desorption and regeneration of PAC@Fe_3O_4 were also accomplished by order to treat the adsorbed metal ion nanocomposite with a 0.1 M solution of HNO_3 and the % desorption was measured using Eq. (2).

$$\%\ desorption = \frac{amount\ of\ metal\ ion\ desorbed\ to\ desorbing\ media}{amount\ of\ metal\ ion\ adsorbed\ on\ adsorbent} \times 100 \tag{2}$$

3 Results and discussion

3.1 Characterization of PAC@Fe_3O_4

3.1.1 SEM with EDX analysis

Figure 1 (a)–(f) depict the surface morphologies of cellulose, PAM, and present nanocomposite PAC@Fe_3O_4 with EDX images before and the after sequestration of Pb(II). The cellulose in the SEM image seems to be fibrous and smooth, whereas the PAM appears to have a flaky surface.

However, after PAM grafting and adding Fe_3O_4 MNPs for reinforcement, the fibrous structure turns into porous substance. After the adsorption of Pb(II), the porous structure becomes footless flakes as a result of water molecule

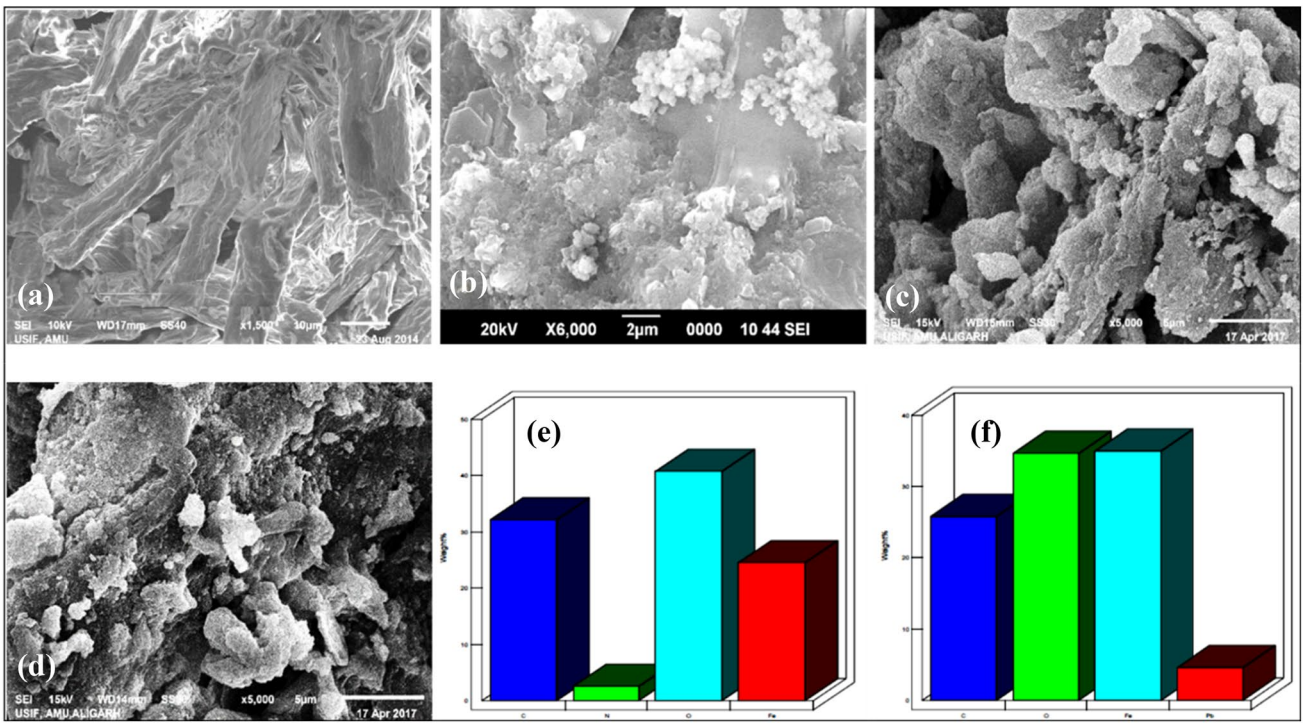

Fig. 1 SEM images of (**a**) cellulose, (**b**) PAM, (**c**) PAC@Fe_3O_4 before adsorption, (**d**) PAC@Fe_3O_4 after adsorption, (**e**) EDX image of PAC@Fe_3O_4 before adsorption, and (**f**) EDX image of PAC@Fe_3O_4 after adsorption

adsorption on the surface shown in Fig. 1(e). The SEM images showed that cellulose was therefore effectively grafted to PAM as in graft copolymer matrix, with reinforcement of Fe_3O_4 MNP nanoparticles.

To recognize the adhesion of Pb(II) ions to the PAC@Fe_3O_4 surface, EDX analysis of PAC@Fe_3O_4 was performed before and after treatment and represented in Fig. 1 (d) and (f). The EDX spectra show the presence of a Pb(II) peak after the adsorption confirmed the Pb(II) adherence to the adsorbent.

3.1.2 TEM analysis

It is indeed difficult to have seen Fe_3O_4 MNPs throughout the nanocomposite matrix because SEM micrographs include a low magnification; thus, using a TEM to observe them in a polymer matrix is an efficient method. The TEM micrograph in Fig. 2 shows that cell@Fe_3O_4 grafted with PAM have produced a nanocomposite with well-distributed nanoparticles in a polymer matrix. As can be seen, the PAM-g-cell matrix uniformly coated Fe_3O_4 MNPs. The average size of nanoparticles was discovered to 20.5 nm.

3.1.3 FTIR

Figure 3 shows the FT-IR spectra of Fe_3O_4 MNPs, exhibits a high absorption peak at 584 cm^{-1} due to Fe–O bond of magnetite [30], and peaks attributed at 1622, 3415 cm^{-1} as a result of stretching and bending vibration of – OH group associated with water. The absorption band observed at 3437 cm^{-1} in the FTIR spectra of PAM identifies amidogen. The bands observed at 2925 cm^{-1} and 1665–1116 cm^{-1} correspond to the symmetric and asymmetric of $-CH_2$ stretching vibration and carboxylate (– COO –) group, N–H vibration, and C–N stretch, respectively [31]. The absorption band of PAC@Fe_3O_4 was aroused at 3404 cm^{-1} to blended – OH stretch vibration of cellulose, PAM, Fe_3O_4, and another peak revealed at 2914 cm^{-1} due to asymmetric and symmetric bending vibrations C–H group from cellulose pyranoid and PAM. A peak appeared at 1665 cm^{-1} which corresponds to bond of carboxylate anions. A band aroused at 1316 cm^{-1} which correspond to (– OH) vibration [32]. The adsorption peaks at 1159–896 cm^{-1} were aroused due to the symmetric stretching of $-CH_2$ group pyranoid ring, anti-symmetric C–O bridge stretch, the cellulose peak to skeletal vibration of C–O–C, and the β-glycosidic linkage, respectively [33]. The band appeared at 562 cm^{-1} corresponds to metal oxide bond. After Pb(II) adsorption in the FTIR spectrum of PAC@Fe_3O_4 show a shift in frequency until a certain point, signifying that the – OH and $-NH_2$ groups are involved in the adsorption.

3.1.4 XRD analysis

XRD patterns of cellulose and PAC@Fe_3O_4 are described in Fig. 4. Diffraction bands of cellulose were obtained at 2θ values of 22.18° and 34.11° [34]. The crystalline nature of the matrix was diminished to a semi-crystalline structure just after grafting and incorporation of Fe_3O_4 MNPs and there revealed some peaks of PAC@Fe_3O_4 nanocomposite in the XRD spectra at 45.31°, 56.88°, and 62.17° that were similar to Fe_3O_4 MNP peaks.

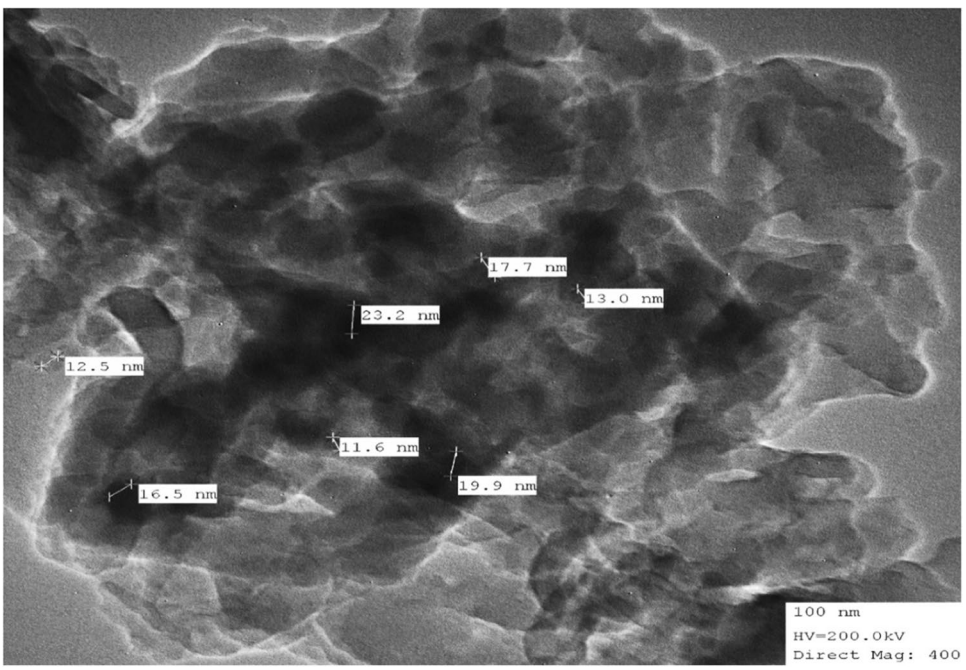

Fig. 2 TEM image of PAC@Fe_3O_4 showing nanoparticle dispersion in the polymer matrix

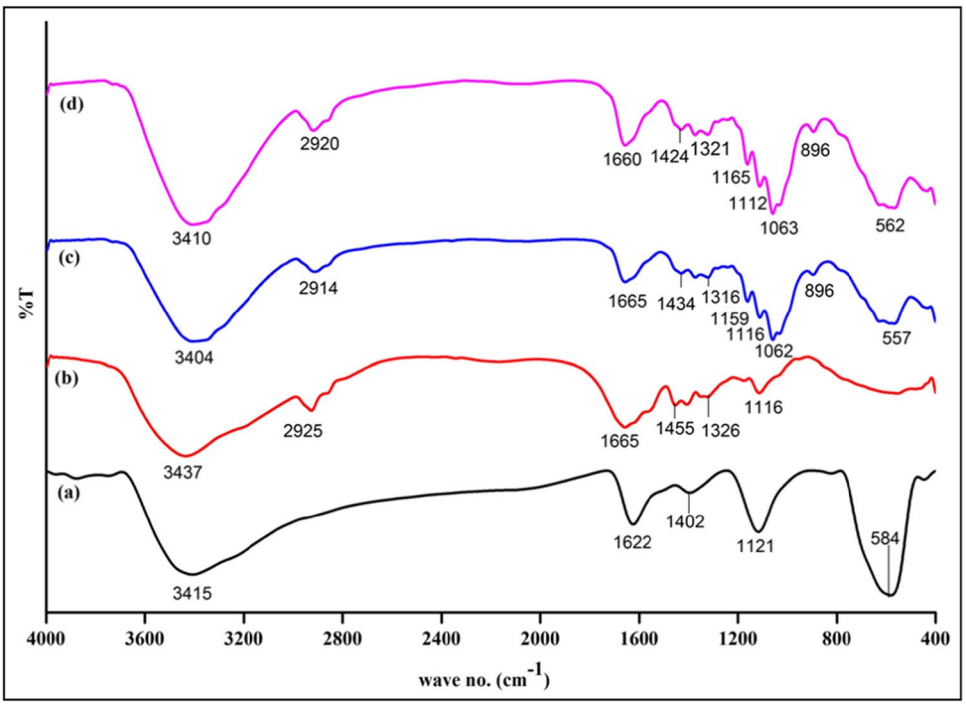

Fig. 3 FTIR spectra of (**a**) Fe_3O_4, (**b**) poly(acrylamide), (**c**) PAC@Fe_3O_4 nanocomposite before adsorption, and (**d**) PAC@Fe_3O_4 nanocomposite after adsorption

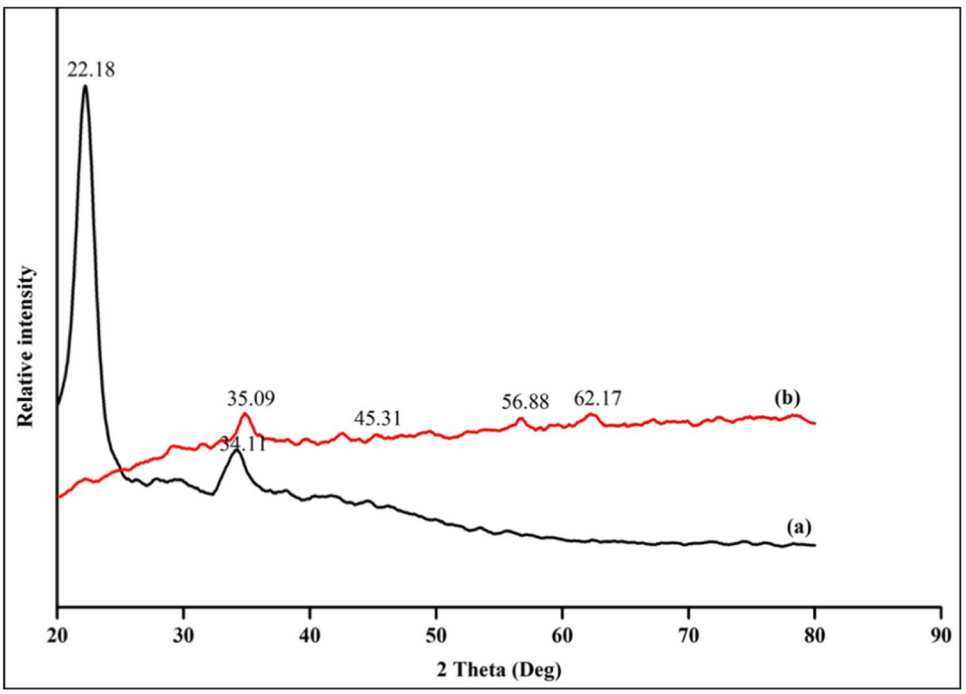

Fig. 4 XRD spectra of (**a**) cellulose and (**b**) PAC@Fe_3O_4

3.2 Adsorption behavior

3.2.1 Influence of pH

The solution pH of adsorbate is a critical factor in adsorption process, and the influence of pH was investigated using pH ranging from 1 to 7 while all other operational parameters were held constant. The impact of pH on Pb(II), Ni(II), and Cu(II) adsorption rates on PAC@Fe_3O_4 is demonstrated in Fig. 5(a). The removal capacity of Pb(II), Ni(II), and Cu(II) increases as pH rises until it reaches a maximum of pH 5 for Pb(II) and Cu(II) while for Ni(II) pH 4 because hydroxyl and carboxylic groups on the surface of PAC@Fe_3O_4 have protonated. While the absorption rate tends to reduce after

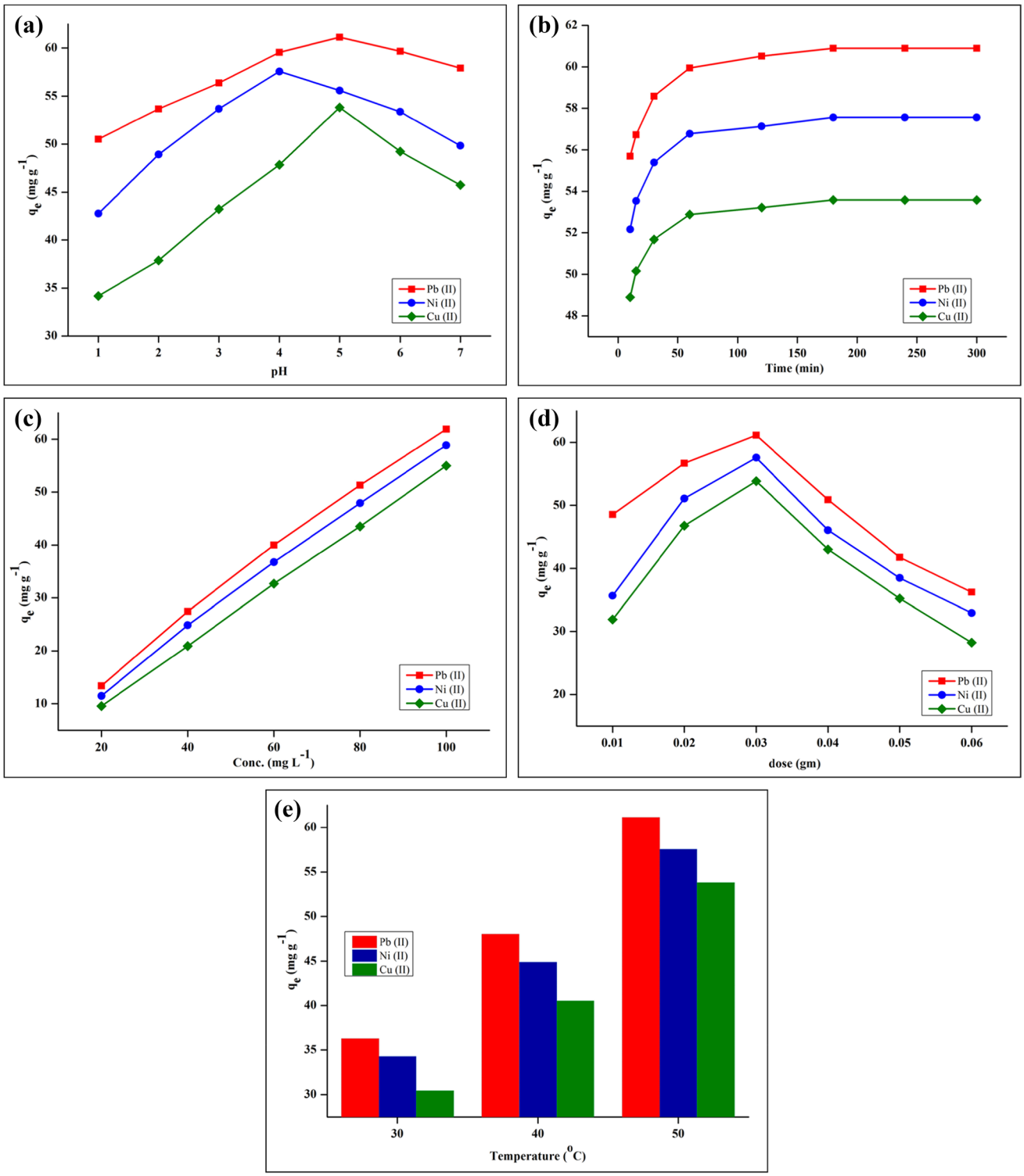

Fig. 5 (**a**) Effect of pH on adsorption of Pd(II), Ni(II), and Cu(II) on PAC@Fe_3O_4 at 100 mg L^{-1} initial metal ion concentration. (**b**) Effect of contact time on adsorption of Pb(II), Ni(II), and Cu(II) on PAC@Fe_3O_4 at 100 mg L^{-1} initial metal ion concentration. (**c**) Effect of initial metal ion concentration on adsorption of Pb(II), Ni(II), and Cu(II) on PAC@Fe_3O_4 at optimum pH. (**d**) Effect of adsorbent dose on adsorption of Pb(II), Ni(II), and Cu(II) on PAC@Fe_3O_4 at 100 mg L^{-1} initial metal ion concentration. (**e**) Effect of temperature on adsorption of Pb(II), Ni(II), and Cu(II) on PAC@Fe_3O_4 at 100 mg L^{-1} initial metal ion concentration

pH 5 due to metal ion functionalization in hydroxides form. As a result, the value of pH 5 was selected as the optimal pH for Pb(II) and Cu(II) while for Ni(II) pH 4 for further studies as maximum capacity of 61.13 mg g^{-1} for Pb(II), 57.56 mg g^{-1} for Ni(II), and 53.83 mg g^{-1} for Cu(II) was found at this pH level and similar results have also been reported elsewhere [35, 36]. The following process is suited to explain mechanism for adsorption of Pb(II), Ni(II), and Cu(II) on synthesized nanocomposite.

$$R-OH + M^{2+} \rightarrow R-O-M^{+} + H^{+} \text{Chemical binding adsorption}$$
$$R-O^{-} + M^{2+} \rightarrow R-O-M^{2+} \text{Electrostatic binding adsorption}$$

3.2.2 Influence of contact time

Influence of time is a vital factor in adsorption experiments because it influences the kinetics of adsorption. Batch studies were carried out to determine the optimum condition for achieving equilibrium time using PAC@Fe_3O_4 with 100 mg L^{-1} solution of adsorbate in a time range 5–300 min. Equation (1) was used to analyze the adsorbed amount of Pb(II), Ni(II), and Cu(II). In Fig. 5(b), these values are plotted against contact time (min). As a result of abundance of active species onto surface of nanocomposite, heavy metal adsorption seems to be very fast in the first 180 min. After reached 180 min, the uptake of Pb(II), Ni(II), and Cu(II) ions has to become slow as an active species decreases, and that no changes in the uptake process are observed. The maximum capacity was obtained as 61.13 mg g^{-1} for Pb(II), 57.56 mg g^{-1} for Ni(II), and 53.83 mg g^{-1} for Cu(II) at 180 min. Therefore, the optimal time for Pb(II), Ni(II), and Cu(II) adsorption was selected as 180 min.

3.2.3 Influence of concentration

The initial metal ion concentration acts as a powerful driving force for accomplishments all metal ion resistance of mass transfer between liquid and the solid phases [37]. To examine the influence of concentration on PAC@Fe_3O_4 adsorption, a series of metal ion concentrations in the range of 20 to 100 mg L^{-1} of adsorbate were selected. The influence of metal concentration is also shown in Fig. 5(c), where the adsorption capacity subsequently increases as the concentration of Pb(II), Ni(II), and Cu(II) ions increases. The maximum removal capacity was observed 61.13 mg g^{-1}, 57.56 mg g^{-1}, and 53.83 mg g^{-1}, respectively, at 100 mg L^{-1} which could be because the number of adsorbent-adsorbate species collisions increased on increasing the concentration of metal ions. This has resulted in a significance in metal accessing [38].

3.2.4 Influence of dose

The amount of adsorbent dose used has a significant impact on metal ion adsorption in the solution. To analyze influence of dose on the sequestration of Pb(II), Ni(II), and Cu(II), the range of doses were used from 0.01 to 0.06 g in 20 mL solution of metal (100 mg L^{-1}) for 180 min and the results are shown in Fig. 5(d). It was discovered that as adsorbent doses increase up to 0.03 g, the removal efficiency of Pb(II), Ni(II), and Cu(II) ions increased but as the amount of dose is increased further, the adsorption capacity decreased. This occurrence can be explained to the fact that as the amount of dose rises, so the number of sorbent molecules rises as well, allowing for more active adsorption sites; however, if the adsorbent dose is increased further, due to partial adhesion of adsorbent molecule, adsorption efficiency decreased. For all of the studies, 0.03 g was selected as optimum adsorbent dose.

3.2.5 Influence of temperature

As shown in Fig. 5(e), influence of temperature on sequestration of Pb(II), Ni(II), and Cu(II) was evaluated between 30 and 50 °C temperature range. It was discovered that as the temperature rises, the removal efficiency rises as well, owing to an increase in the rate of metal ion diffusion between the external layer of boundary and inside the pores of PAC@Fe_3O_4 nanocomposite. Moreover, the energy of structure helped facilitate for the binding of adsorbate at high temperature signifying that Pb(II), Ni(II), and Cu(II) adsorption onto PAC@Fe_3O_4 surface is an endothermic process. As a result, for all adsorption studies, the optimal temperature was selected as 50 °C.

3.3 Adsorption isotherms

The isotherm adsorption studies for explaining the concentrations have an influence on adsorbate adsorbed onto adsorbent surface, resulting to efficient adsorption equilibrium condition. In this study, various isotherm parameters, namely, Langmuir model, Freundlich isotherm, Temkin, and Redlich-Peterson model, were used to analyze the results of the experiment.

3.3.1 Langmuir isotherm model

The Langmuir parameter is a reversible chemical equilibrium that describes the state of the surface of a solid and its solution is in equilibrium. The Langmuir isotherm parameter works well for the adsorption on such a surface with the limited number of functional sites. Langmuir method

is founded on the statement that a saturated surface layer of solute particles on the active sites corresponds to a maximum adsorption, which is represented as follows:

$$q_e = \frac{q_m K_L C_e}{1 + K_L C_e} \tag{3}$$

where q_m (mg g^{--1}) and K_L (L mg^{-1}) denote the maximum adsorption capacity and Langmuir constant, respectively. The values of q_m and K_L are listed in Table 1. In order to predict whether adsorption process is favorable or unfavorable, R_L, a constant with no dimensions mentioned to as a separation factor, was also calculated. R_L is determined by the following equation:

$$R_L = \frac{1}{1 + K_L C_o} \tag{4}$$

where C_o denotes initial adsorbate concentration (mg L^{-1}). The values of constant R_L confirm the adsorption favorability as follows:

$R_L > 1$, unfavorable adsorption
$0 < R_L < 1$, favorable adsorption
$R_L = 0$, irreversible adsorption
$R_L = 1$, linear adsorption

As shown in Fig. 6(a), the non-linear curve for Langmuir isotherm was obtained for Pb(II), Ni(II), and Cu(II) by non-linear regression analysis. The isotherm results are reported in Table 1; the maximum adsorption capacities (q_m) were found to be 313.02, 219.33, and 210.71 mg g^{-1} for Pb(II), Ni(II), and Cu(II) at 50 °C. The regression coefficient and χ^2 values for Pb(II), Ni(II), and Cu(II) are 0.99, 0.99, and 0.99 and are 1.41, 1.22, and 0.29, respectively, which indicates that the Langmuir isotherm is best followed for Pb(II), Ni(II), and Cu(II) removal with equilibrium data.

Table 1 Isotherm parameters for Pb(II), Ni(II), and Cu(II) removal by PAC@Fe_3O_4 at 50 °C

Model	Parameters	Metal Ions		
		Pb(II)	Ni(II)	Cu(II)
Langmuir	q_m (mg g^{-1})	313.02	219.33	210.71
	K_L (L mg^{-1})	0.102	0.018	0.003
	R_2	0.99	0.99	0.99
	χ^2	1.41	1.22	0.29
Freundlich	n	1.55	1.20	1.04
	K_L (mg g^{-1})	13.02	4.97	2.38
	R_2	0.98	0.99	0.99
	χ^2	3.72	3.15	0.19
Temkin	A_T (L mg^{-1})	1.28	0.40	0.28
	b_T (J mol^{-1})	115.76	94.01	103.02
	R^2	0.97	0.97	0.97
	χ^2	8.22	8.51	6.26
Redlich–Peterson	g	1.61	5.74	5.95
	K_R (L g^{-1})	11.27	5.88	2.10
	a_R (L mg^{-1})	0.47	4.49	1.26
	R^2	0.96	0.98	0.99
	χ^2	13.99	5.64	0.81

3.3.2 Freundlich isotherm

The Freundlich model is the first adequate model on the basis of reversible complex surface adsorption. The following equation is used to explain the model:

$$q_e = K_F C_e^{1/n} \tag{5}$$

where K_F ((mg g^{-1}) (L mg^{-1})$^{1/n}$) is a capacity constant and $1/n$ is the adsorption intensity. The obtained value of n greater than 1 indicates that the adsorption conditions are favorable [39]. The constant n and K_F values are attained from a non-linear graph of q_e against C_e as illustrated in Fig. 6(b). Freundlich constant (n) values between 1 and 10 are associated with favorable adsorption. A higher n value (> 1) denotes a strong interaction between the adsorbate and adsorbent while ($1/n = 1$) signifies linear adsorption, which results in identical adsorbed species for all sites. Table 1 shows that for sequestration of Pb(II), Ni(II), and Cu(II), the values of n are greater than 1, signifying favorable adsorption.

3.3.3 Temkin isotherm

Adsorption heat is taken into account in the Temkin model, which decreases linearly as the metal ions and nanocomposite interactions are covered. The Temkin model has been applied in the following terms:

$$q_e = B\ln(AC_e) \tag{6}$$

$$B = \frac{RT}{b} \tag{7}$$

where R (J mol^{-1} K^{-1}) and T (K) denote the gas constant and absolute temperature, respectively. b_T (J mol^{-1}) and A_T (L g^{-1}) are Temkin constants corresponding to adsorption heat and maximal binding energy. The non-liner curve of q_e versus C_e shown in Fig. 6(c) helps to define constant terms A_T and b_T. The values of Temkin constant from Table 1 signify that the adsorption is due to chemisorption of Pb(II), Ni(II), and Cu(II) as well as a mechanism for ion exchange. The Temkin model provides a better fitted with data of all studied metal ions. The high affiliation of Pb(II), Ni(II), and Cu(II) more toward the adsorbent surface is also supported by the values of binding constant A_T reported in Table 1.

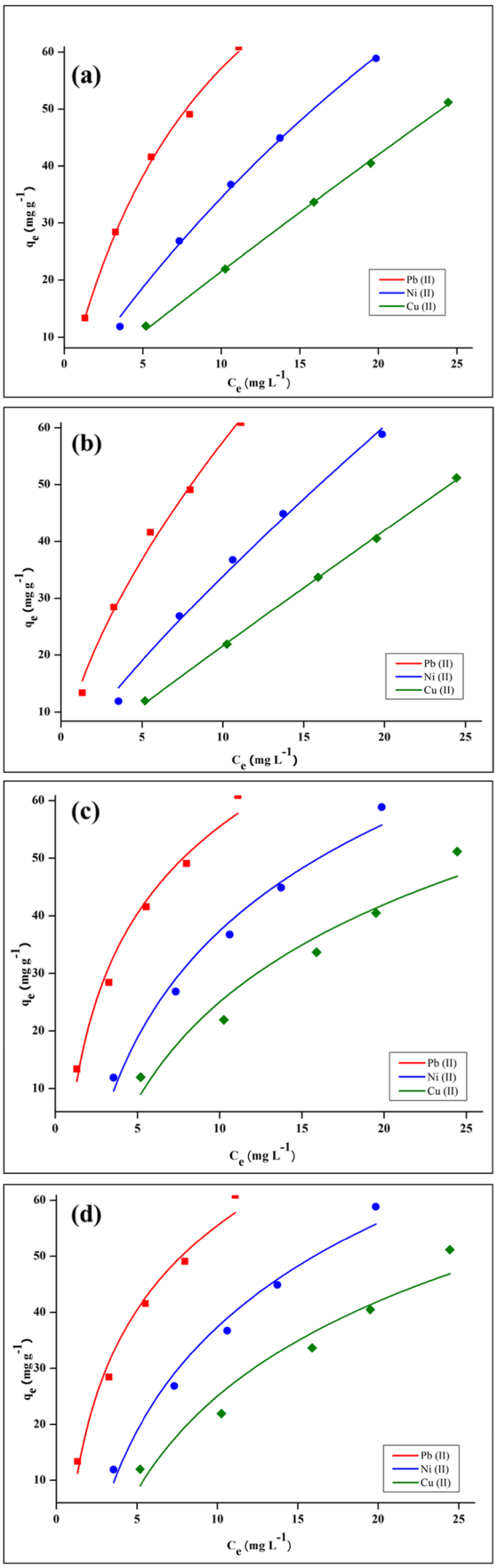

Fig. 6 (**a**) Langmuir adsorption isotherm for Pb(II), Ni(II), and Cu(II) on PAC@Fe_3O_4 at 50 °C (dose = 0.03 g and optimum pH). (**b**) Freundlich adsorption isotherm for Pb(II), Ni(II), and Cu(II) on PAC@Fe_3O_4 at 50 °C (dose = 0.03 g and optimum pH). (**c**) Temkin adsorption isotherm for Pb(II), Ni(II), and Cu(II) on PAC@Fe_3O_4 at 50 °C (dose = 0.03 g and optimum pH). (**d**) Redlich-Peterson adsorption isotherm for Pb(II), Ni(II), and Cu(II) on PAC@Fe_3O_4 at 50 °C (dose = 0.03 g and optimum pH)

3.3.4 Redlich-Peterson isotherm

For the Redlich-Peterson model, a non-linear equation is given:

$$q_e = \frac{K_R C_e}{1 + a_R C_e^g} \tag{8}$$

where the term K_R (L g^{-1}) and a_R (L mg^{-1}) denote the constants for *R-P* isotherm and g is a positive exponent with a value ranging from 0 to 1. The exponent value of g computed by *R-P* isotherm model (Fig. 6(d)) is equal to unity shown in Table 1, suggesting that the Langmuir isotherm is best described with equilibrium data.

3.4 Adsorption kinetics

The measurement of kinetic models for sequestration method is a prerequisite for applying adsorption at a larger scale. The experimental data were attempted to explain by Lagergren pseudo-first order [40] and pseudo-second order [41] in determining the mechanism that governs the adsorption technique. The non-linear equations (Eqs. (9) and (10)) for these kinetic models are as follows:

$$q_t = q_e(1 - e^{-k_1 t}) \tag{9}$$

$$q_t = \frac{k_2 q_e^2 t}{1 + k_2 q_e t} \tag{10}$$

where q_e (mg g^{-1}) is adsorbed amount of adsorbate at equilibrium time and q_t (mg g^{-1}) at contact time (t), while k_1 (min^{-1}) and k_2 (g mg^{-1} min^{-1}) are constant for pseudo-first order and pseudo-second order.

Figure 7 (a), (b) show the equilibrium data from the sequestration of Pb(II), Ni(II), and Cu(II) onto the present nanocomposite at optimal pH, concentration (100 mg L^{-1}) and temperature (50 °C). The variables for kinetic models, R^2 and χ^2 observed using non-linear equation of kinetic parameters, are reported in Table 2. It is apparent to see that the values of R^2 (0.98, 0.99, and 0.99) are relatively large with low values of χ^2 (0.09, 0.04, and 0.03) for pseudo second kinetic model as shown in Fig. 7(b) followed by pseudo-first order (R^2 = 0.67, 0.74, and 0.73) and (χ^2 = 1.38, 1.14, and

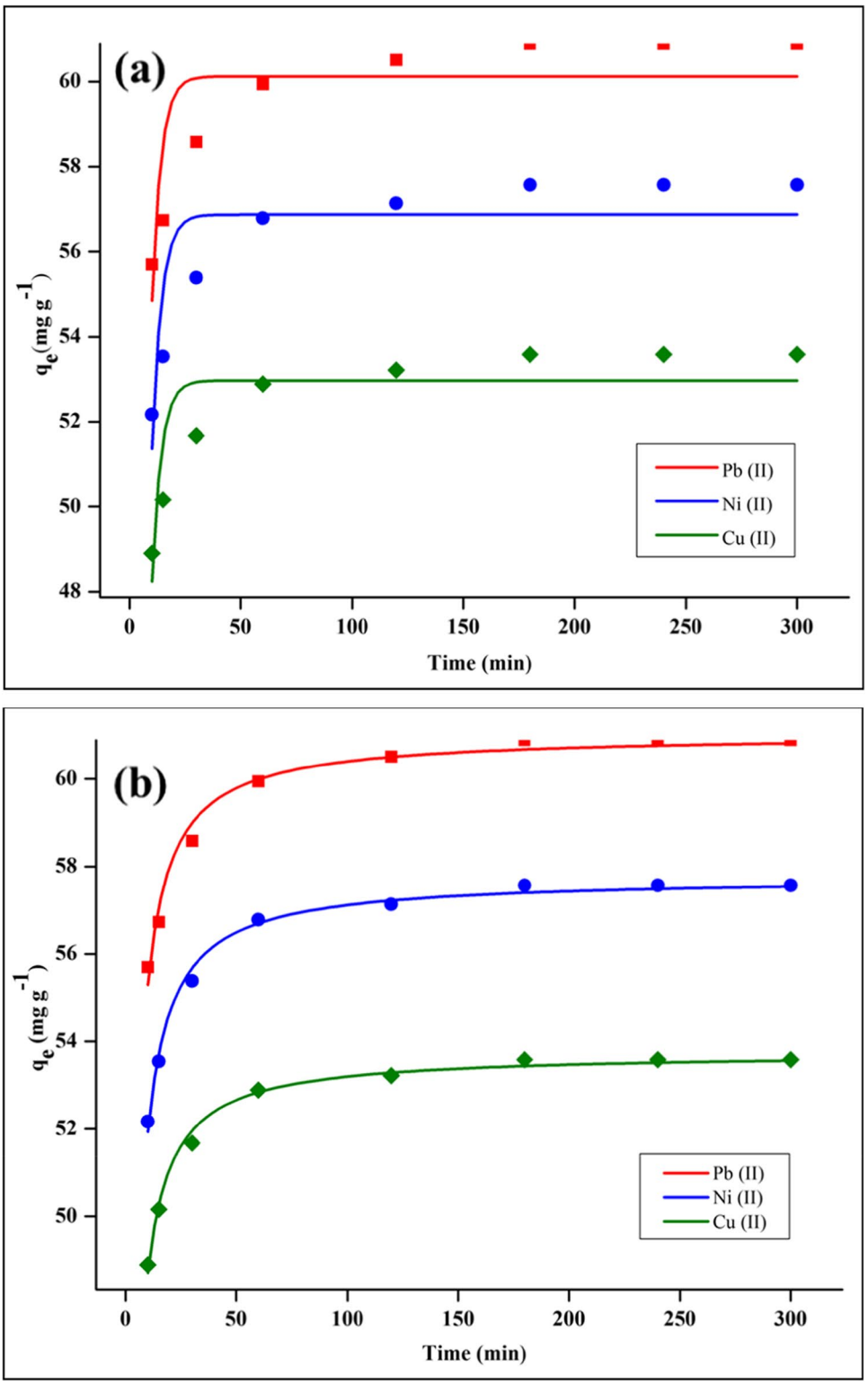

Fig. 7 (**a**) Non-linear Pseudo-first-order plot for Pb(II), Ni(II), and Cu(II) on PAC@Fe_3O_4 at 50 °C (dose = 0.03 g and optimum pH). (**b**) Non-linear pseudo-second-order plot for Pb(II), Ni(II), and Cu(II) on PAC@Fe_3O_4 at 50 °C (dose = 0.03 g and optimum pH)

0.86) in Fig. 7(a). Meanwhile, $q_{e,\,cal}$ values (61.02, 57.76, and 53.74 mg g^{-1}) found from equation of pseudo second model are discovered to approve mildly with values of $q_{e,\,exp}$ (61.13, 57.56, and 53.83 mg g^{-1}). The value $q_{e,\,cal}$ (60.12, 56.86, and 52.97 mg g^{-1}) estimated from the pseudo-first kinetic equation has a least agreement with $q_{e,\,exp}$ (61.13, 57.56, and 53.83 mg g^{-1}). So, the adsorption experiment for Pb(II), Ni(II), and Cu(II) onto PAC@Fe_3O_4 can be most accurately defined by kinetic model of pseudo-second order with the chemisorption as the rate limiting step.

Table 2 Kinetic parameters for Pb(II), Ni(II), and Cu(II) removal by PAC@Fe_3O_4 at 50 °C obtained through non-linear regression analysis

Model	Parameters	Metal ions		
		Pb(II)	Ni(II)	Cu(II)
Pseudo-first order	q_e (exp) (mg g^{-1})	61.13	57.56	53.83
	q_e (cal) (mg g^{-1})	60.12	56.86	52.97
	k_1 (min^{-1})	0.24	0.23	0.24
	R^2	0.67	0.74	0.73
	χ^2	1.38	1.14	0.86
Pseudo-second order	q_e (exp) (mg g^{-1})	61.13	57.56	53.83
	q_e (cal) (mg g^{-1})	61.02	57.76	53.74
	k_2 (g mg^{-1} min^{-1})	0.01	0.01	0.02
	R^2	0.98	0.99	0.99
	χ^2	0.09	0.04	0.03

3.5 Adsorption thermodynamics

A series of experiment were performed to validate our statement that the adsorption process is endothermic. The parameters for thermodynamic like enthalpy change ($\Delta H°$), Gibbs free energy change ($\Delta G°$), and entropy change ($\Delta S°$) were analyzed by using Gibbs and Van't Hoff equation [42], listed as follows:

$$\Delta G^0 = -RTlnK_C \tag{11}$$

Table 3 Thermodynamic parameters for Pb(II), Ni(II), and Cu(II) removal by PAC@Fe_3O_4

Metal ions	$\Delta H°$ (KJ mol^{-1})	$\Delta S°$ (KJ mol^{-1} K^{-1})	$\Delta G°$ (KJ mol^{-1})		
			30 °C	40 °C	50 °C
Pb(II)	9.87	0.052	−5.91	−6.41	−6.96
Ni(II)	6.70	0.037	−4.64	−4.96	−5.39
Cu(II)	4.50	0.026	−3.55	−3.80	−4.08

$$\ln K_C = -\frac{\Delta H^0}{RT} + \frac{\Delta S^0}{R} \tag{12}$$

where R and T denote the gas constant (J mol^{-1} K^{-1}) and absolute temperature (K) and K_c is the distribution factor. The values of $\Delta G°$ and $\Delta S°$ were calculated by using plot ln K_c versus $1/T$, as depicted in Fig. 8. The equation below was used to calculate the free energy change ($\Delta G°$):

$$\Delta G^o = \Delta H^o - T\Delta S^0 \tag{13}$$

The thermodynamic studies identified with the sequestration of metal ions using PAC@Fe_3O_4 nanocomposite are tabulated in Table 3. The fact that $\Delta H°$ was positive indicated that the adsorption process for Pb(II), Ni(II), and Cu(II) onto PAC@Fe_3O_4 was endothermic. The Gibbs energy ($\Delta G°$) has all the values negative and increases with increasing temperature from 30 to 50 °C, which demonstrates that the

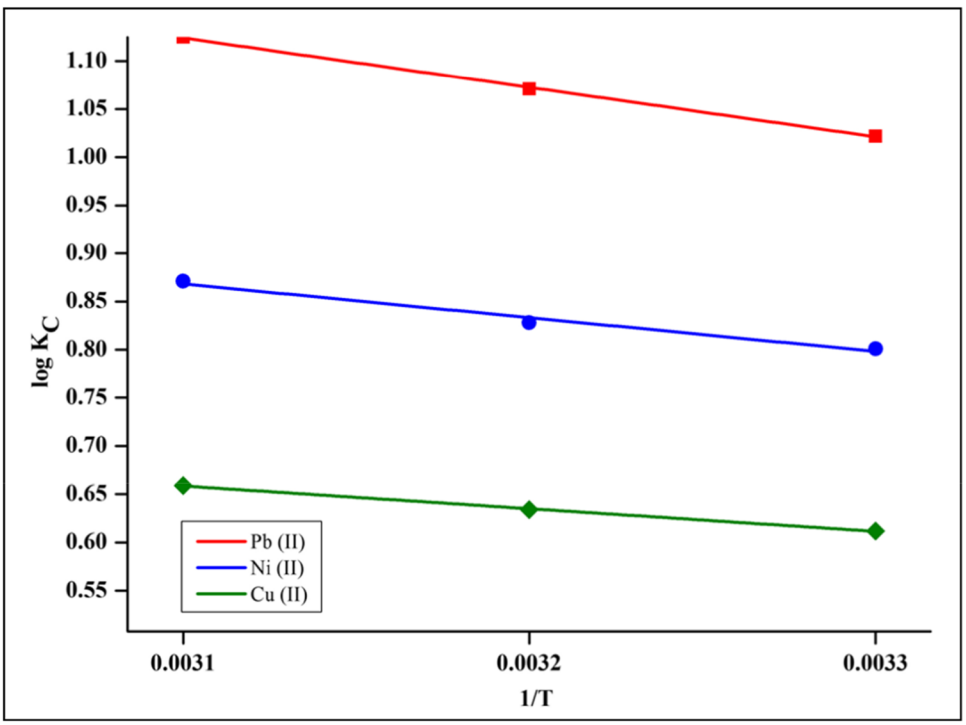

Fig. 8 Thermodynamic plot for removal of Pb(II), Ni(II), and Cu(II) on PAC@Fe_3O_4 at 30, 40, and 50 °C

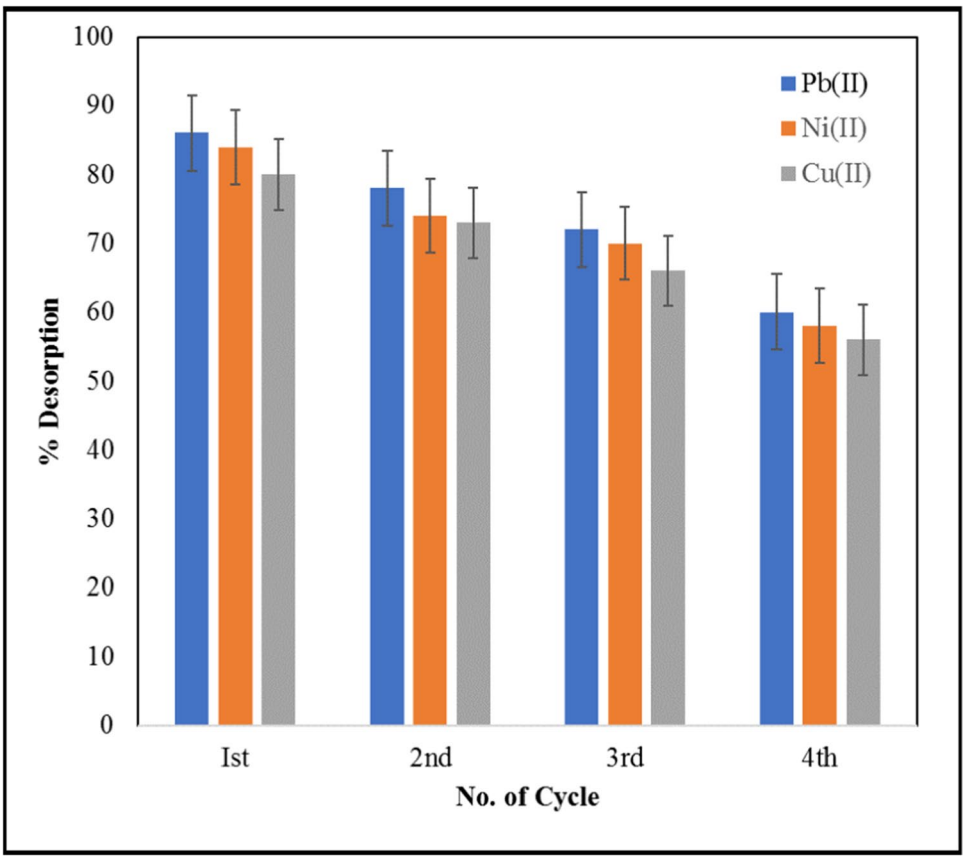

Fig. 9 Desorption studies of Pb(II), Ni(II), and Cu(II) on exhausted PAC@Fe_3O_4 by 0.1 M HNO_3

sequestration of Pb(II), Ni(II), and Cu(II) onto synthesized nanocomposite is spontaneous nature and temperature causes spontaneity to increase [43]. As during immobility of adsorbate on the effective sites on the surface of nanocomposite, at the adsorption process the positive value of $\Delta S°$ showed greater randomness and degrees of freedom, which declare that the salvation metal ions are partially liberated as from adsorbate particles before adsorption (water molecules are liberated from solvated toxic metals), as a result, allowing for the commonality of randomness and spontaneity in the method.

Table 4 Comparison of Pb(II), Ni(II), and Cu(II) adsorption capacity with various other adsorbents

Pollutant	Adsorbents	q_{max} (mg g^{-1})	References
Pb(II)	Pyromellitic acid modified-UiO-66-NH2	226.1	[44]
	Xanthan gum-glutathione/zeolite bionanocomposite	109.07	[45]
	Chitosan functionalized dialdehyde viscose fiber	207	[46]
	PMDA-PGMA	206.72	[47]
	PAC@Fe_3O_4 nanocomposite	313.02	This study
Ni(II)	Xanthan gum-glutathione/zeolite bionanocomposite	101.27	[45]
	COPR	18.21	[48]
	HAp	9.53	[49]
	CS-AOPAM	213.4	[50]
	PAC@Fe_3O_4 nanocomposite	219.33	This study
Cu(II)	HAp	10.58	[49]
	CS-AOPAM	215.5	[50]
	MPCB	69.8	[51]
	GSC	2.76	[52]
	PAC@Fe_3O_4 nanocomposite	210.71	This study

3.6 Desorption and regeneration

To make entire process more feasible and cost-effective, the exhausted PAC@Fe_3O_4 nanocomposite was desorbed with 0.1 M solution of HNO_3. Figure 9 shows that adsorbed metal ions of Pb(II), Ni(II), and Cu(II) can desorb 86, 84, and 80%, respectively, from the spent PAC@Fe_3O_4 nanocomposite. The PAC@Fe_3O_4 nanocomposite was further regenerated up to 4th cycle successfully without significant loss in capacity, and this makes it a potential adsorbent to remove metal ions from aqueous solution and wastewater economically.

3.7 Comparison with another adsorbent

A comparison of capacities of PAC@Fe_3O_4 nanocomposite onto Pb(II), Ni(II), and Cu(II) metal ions with other adsorbents is tabulated in Table 4. The present nanocomposite gives better capacity for sequestration of Pb(II), Ni(II), and Cu(II) as compared with other adsorbents reported in literature table.

4 Conclusions

In this work, poly(acrylamide)-grafted cell@Fe_3O_4 nanocomposite was prepared by polymerizing acrylamide monomer with oxidative free radicals in the existing cell@Fe_3O_4 nanoparticles. Various types of analytical methods such as XRD, TEM, SEM, and FTIR were used to characterize the material. The nanocomposite material was also investigated for its ability to remove Pb(II), Ni(II), and Cu(II) from wastewater. The sequestration of heavy metal is depending on the pH, and the highest monolayer capacities for studied metal ions were acquired at pH 5 for Pb(II) and Cu(II) while pH 4 for Ni(II). The various isotherm parameters were utilized to evaluate the equilibrium data, and concluded that the Langmuir isotherm was best followed model with data. The maximal adsorption capacity was measured to be 313.02 mg g^{-1} for Pb(II), 219.33 mg g^{-1} for Ni(II), and 210.71 mg g^{-1} for Cu(II), respectively. The adsorption of heavy metals by PAC@Fe_3O_4 followed a kinetic model of pseudo-second order, with chemisorption being the rate-limiting step, according to all kinetic parameters. In nature, the adsorption is endothermic and spontaneous concluded by positive ΔH° value and negative ΔG° value. The nanocomposite was regenerated up to 4th cycle successfully without much loss in capacity. The above results confirmed that the present nanocomposite can be successfully used for adsorption of toxic metal ions such as Pb(II), Ni(II), and Cu(II) from industrial waste water.

Acknowledgements The authors are grateful for research facilities to the Chairman, Department of Applied Chemistry, AMU, Aligarh, India; USIF for SEM, TEM, and EDX facility and Department of Physics; and AMU for XRD.

Author contribution Rais Ahmad: conceptualization, visualization, resources, data curation, writing—review and editing, supervision.

Khalid Ansari: investigation, methodology, validation, and writing—original draft.

Mohammad Osama Ejaz: formal analysis, software.

Declarations

Conflict of interest The authors declare no competing interests.

References

1. M. Kebir, M. Chabani, N. Nasrallah, A. Bensmaili, M. Trari, Coupling adsorption with photocatalysis process for the Cr(VI) removal. Desalination **270**, 166–173 (2011). https://doi.org/10.1016/j.desal.2010.11.041
2. O. Bičáková, P. Straka, Production of hydrogen from renewable resources and its effectiveness. Int. J. Hydrogen Energy **37**, 11563–11578 (2012). https://doi.org/10.1016/j.ijhydene.2012.05.047
3. J. Wang, C. Chen, Biosorbents for heavy metals removal and their future. Biotechnol. Adv. **27**, 195–226 (2009). https://doi.org/10.1016/j.biotechadv.2008.11.002
4. M.A. Hashim, S. Mukhopadhyay, J.N. Sahu, B. Sengupta, Remediation technologies for heavy metal contaminated groundwater. J. Environ. Manage. **92**, 2355–2388 (2011). https://doi.org/10.1016/j.jenvman.2011.06.009
5. D. Kavak, Removal of lead from aqueous solutions by precipitation: statistical analysis and modeling. Desalin. Water Treat. **51**, 1720–1726 (2013). https://doi.org/10.1080/19443994.2012.714652
6. M.R. Awual, M.M. Hasan, A. Shahat, Functionalized novel mesoporous adsorbent for selective lead(II) ions monitoring and removal from wastewater. Sens. Actuators, B Chem. **203**, 854–863 (2014). https://doi.org/10.1016/j.snb.2014.07.063
7. Y. Ren, N. Li, J. Feng, T. Luan, Q. Wen, Z. Li, M. Zhang, Adsorption of Pb(II) and Cu(II) from aqueous solution on magnetic porous ferrospinel $MnFe_2O_4$. J. Colloid Interface Sci. **367**, 415–421 (2012). https://doi.org/10.1016/j.jcis.2011.10.022
8. L. Yuan, Y. Liu, Removal of Pb(II) and Zn(II) from aqueous solution by ceramisite prepared by sintering bentonite, iron powder and activated carbon. Chem. Eng. J. **215–216**, 432–439 (2013). https://doi.org/10.1016/j.cej.2012.11.016
9. R. Ahmad, K. Ansari, Enhanced sequestration of methylene blue and crystal violet dye onto green synthesis of pectin modified hybrid (Pect/AILP-Kal) nanocomposite. Process Biochem. **111**(2), 132–143 (2021). https://doi.org/10.1016/j.procbio.2021.10.009
10. C.-V. Gherasim, J. Křivčík, P. Mikulášek, Investigation of batch electrodialysis process for removal of lead ions from aqueous solutions. Chem. Eng. J. **256**, 324–334 (2014). https://doi.org/10.1016/j.cej.2014.06.094
11. F. Fu, L. Xie, B. Tang, Q. Wang, S. Jiang, Application of a novel strategy—advanced Fenton-chemical precipitation to the treatment of strong stability chelated heavy metal containing wastewater. Chem. Eng. J. **189–190**, 283–287 (2012). https://doi.org/10.1016/j.cej.2012.02.073

12. R. Ahmad, K. Ansari, Chemically treated Lawsonia inermis seeds powder (CTLISP): an eco-friendly adsorbent for the removal of brilliant green dye from aqueous solution, Groundw. Sustain. Dev. **11**, 100417 (2020). https://doi.org/10.1016/j.gsd.2020.100417
13. R. Yadav, T. Baskaran et al., Recent advances in the preparation and applications of organo-functionalized porous materials. Chem. Asian J. **15**, 2588–2621 (2020). https://doi.org/10.1002/asia.202000651
14. L. Li, Y. Li, C. Yang, Chemical filtration of Cr (VI) with electrospun chitosan nanofiber membranes. Carbohyd. Polym. **140**, 299–307 (2016). https://doi.org/10.1016/j.carbpol.2015.12.067
15. E. Eren, Removal of copper ions by modified Unye clay, Turkey. J. Hazard. Mater. **159**, 235–244 (2008). https://doi.org/10.1016/j.jhazmat.2008.02.035
16. G. Crini, Recent developments in polysaccharide-based materials used as adsorbents in wastewater treatment. Prog. Polym. Sci. **30**, 38–70 (2005). https://doi.org/10.1016/j.progpolymsci.2004.11.002
17. P.J. Manna, T. Mitra, N. Pramanik, V. Kavitha, A. Gnanamani, P.P. Kundu, Potential use of curcumin loaded carboxymethylated guar gum grafted gelatin film for biomedical applications. Int. J. Biol. Macromol. **75**, 437–446 (2015). https://doi.org/10.1016/j.ijbiomac.2015.01.047
18. V. Vijan, S. Kaity, S. Biswas, J. Isaac, A. Ghosh, Microwave assisted synthesis and characterization of acrylamide grafted gellan, application in drug delivery. Carbohyd. Polym. **90**, 496–506 (2012). https://doi.org/10.1016/j.carbpol.2012.05.071
19. X. Yu, S. Tong, M. Ge, J. Zuo, Removal of fluoride from drinking water by cellulose@hydroxyapatite nanocomposites. Carbohyd. Polym. **92**, 269–275 (2013). https://doi.org/10.1016/j.carbpol.2012.09.045
20. X. Chen, C. Burger, F. Wan, J. Zhang, L. Rong, B.S. Hsiao, B. Chu, J. Cai, L. Zhang, Structure study of cellulose fibers wet-spun from environmentally friendly NaOH/urea aqueous solutions. Biomacromol **8**, 1918–1926 (2007). https://doi.org/10.1021/bm061186i
21. K. Bredereck, F. Hermanutz, Man-made cellulosics. Rev. Prog. Color. Relat. Top. **35**, 59–75 (2008). https://doi.org/10.1111/j.1478-4408.2005.tb00160.x
22. T.-Y. Kim, Y. Yamazaki, T. Hirano, Magneto-optical properties of Bi-YIG nanoparticle with polymethacrylate matrix materials. Phys. Stat. Sol. (B) **241**, 1601–1604 (2004). https://doi.org/10.1002/pssb.200304511
23. L. Qin, X.-W. He, W.-Y. Li, Y.-K. Zhang, Molecularly imprinted polymer prepared with bonded β-cyclodextrin and acrylamide on functionalized silica gel for selective recognition of tryptophan in aqueous media. J. Chromatogr. A **1187**, 94–102 (2008). https://doi.org/10.1016/j.chroma.2008.02.004
24. Q. Li, M.H.W. Lam, R.S.S. Wu, B. Jiang, Rapid magnetic-mediated solid-phase extraction and pre-concentration of selected endocrine disrupting chemicals in natural waters by poly(divinylbenzene-co-methacrylic acid) coated Fe_3O_4 core-shell magnetite microspheres for their liquid chromatography–ta. J. Chromatogr. A **1217**, 1219–1226 (2010). https://doi.org/10.1016/j.chroma.2009.12.035
25. S. Ghorai, A. Sinhamahpatra, A. Sarkar, A.B. Panda, S. Pal, Novel biodegradable nanocomposite based on XG-g-PAM/SiO_2: application of an efficient adsorbent for Pb^{2+} ions from aqueous solution. Biores. Technol. **119**, 181–190 (2012). https://doi.org/10.1016/j.biortech.2012.05.063
26. F. An, X. Feng, B. Gao, Adsorption mechanism and property of a novel adsorption material PAM/SiO_2 towards 2,4,6-trinitrotoluene. J. Hazard. Mater. **168**, 352–357 (2009). https://doi.org/10.1016/j.jhazmat.2009.02.042
27. S. Zhou, A. Xue, Y. Zhao, Q. Wang, Y. Chen, M. Li, W. Xing, Competitive adsorption of Hg^{2+}, Pb^{2+} and Co^{2+} ions on polyacrylamide/attapulgite. Desalination **270**, 269–274 (2011). https://doi.org/10.1016/j.desal.2010.11.055
28. D. Hritcu, D. Humelnicu, G. Dodi, M.I. Popa, Magnetic chitosan composite particles: evaluation of thorium and uranyl ion adsorption from aqueous solutions. Carbohyd. Polym. **87**, 1185–1191 (2012). https://doi.org/10.1016/j.carbpol.2011.08.095
29. Y. Mansoori, S.V. Atghia, M.R. Zamanloo, G. Imanzadeh, M. Sirousazar, Polymer–clay nanocomposites: free-radical grafting of polyacrylamide onto organophilic montmorillonite. Eur. Polymer J. **46**, 1844–1853 (2010). https://doi.org/10.1016/j.eurpolymj.2010.07.006
30. Z. Yang, X. Gong, C. Zhang, Recyclable Fe_3O_4/hydroxyapatite composite nanoparticles for photocatalytic applications. Chem. Eng. J. **165**, 117–121 (2010). https://doi.org/10.1016/j.cej.2010.09.001
31. Q. Wen, Z. Chen, Y. Zhao, H. Zhang, Y. Feng, Biodegradation of polyacrylamide by bacteria isolated from activated sludge and oil-contaminated soil. J. Hazard. Mater. **175**, 955–959 (2010). https://doi.org/10.1016/j.jhazmat.2009.10.102
32. S. Ali, M.S. Tanweer, M. Alam, Kinetic, isothermal, thermodynamic and adsorption studies on *Mentha piperita* using ICP-OES. Surf. Interfaces. **19**, 100516 (2020). https://doi.org/10.1016/j.surfin.2020.100516
33. W. Lan, C.-F. Liu, F.-X. Yue, R.-C. Sun, J.F. Kennedy, Ultrasound-assisted dissolution of cellulose in ionic liquid. Carbohyd. Polym. **86**, 672–677 (2011). https://doi.org/10.1016/j.carbpol.2011.05.013
34. H.-Z. Song, Z.-Q. Luo, C.-Z. Wang, X.-F. Hao, J.-G. Gao, Preparation and characterization of bionanocomposite fiber based on cellulose and nano-SiO_2 using ionic liquid. Carbohyd. Polym. **98**, 161–167 (2013). https://doi.org/10.1016/j.carbpol.2013.05.079
35. I. Mobasherpour, E. Salahi, M. Pazouki, Comparative of the removal of Pb^{2+}, Cd^{2+} and Ni^{2+} by nano crystallite hydroxyapatite from aqueous solutions: adsorption isotherm study. Arab. J. Chem. **5**, 439–446 (2012). https://doi.org/10.1016/j.arabjc.2010.12.022
36. S.B. Chen, Y.B. Ma, L. Chen, K. Xian, Adsorption of aqueous Cd^{2+}, Pb^{2+}, Cu^{2+} ions by nano-hydroxyapatite: single- and multi-metal competitive adsorption study. Geochem. J. **44**, 233–239 (2010). https://doi.org/10.2343/GEOCHEMJ.1.0065
37. A. Pal, K. Majumder, A. Bandyopadhyay, Surfactant mediated synthesis of poly(acrylic acid) grafted xanthan gum and its efficient role in adsorption of soluble inorganic mercury from water. Carbohyd. Polym. **152**, 41–50 (2016). https://doi.org/10.1016/j.carbpol.2016.06.064
38. A. Pal, A. Giri, A. Bandyopadhyay, Influence of hydrodynamic size and zeta potential of a novel polyelectrolyte poly(acrylic acid) grafted guar gum for adsorption of Pb(II) from acidic waste water, Journal of Environmental. Chem. Eng. **4**, 1731–1742 (2016). https://doi.org/10.1016/j.jece.2016.02.034
39. R. Ahmad, K. Ansari, Polyacrylamide-grafted *Actinidia deliciosa* peels powder (PGADP) for the sequestration of crystal violet dye: isotherms, kinetics and thermodynamic studies. Appl Water Sci **10**, 195 (2020). https://doi.org/10.1007/s13201-020-01263-7
40. A.S. Sartape, A.M. Mandhare, V.V. Jadhav, P.D. Raut, M.A. Anuse, S.S. Kolekar, Removal of malachite green dye from aqueous solution with adsorption technique using *Limonia acidissima* (wood apple) shell as low cost adsorbent. Arab. J. Chem. **10**, S3229–S3238 (2017). https://doi.org/10.1016/j.arabjc.2013.12.019
41. Y. Ho, Review of second-order models for adsorption systems. J. Hazard. Mater. **136**, 681–689 (2006). https://doi.org/10.1016/j.jhazmat.2005.12.043
42. A. Mittal, R. Ahmad, I. Hasan, Poly (methyl methacrylate)-grafted alginate/Fe_3O_4 nanocomposite: synthesis and its application for

the removal of heavy metal ions. Desalin. Water Treat. **57**, 19820–19833 (2016). https://doi.org/10.1080/19443994.2015.1104726
43. R. Ahmad, K. Ansari, Comparative study for adsorption of congo red and methylene blue dye on chitosan modified hybrid nanocomposite. Process Biochem. **108**, 90–102 (2021). https://doi.org/10.1016/j.procbio.2021.05.013
44. Z. Huang, C. Wang, J. Zhao, S. Wang, Y. Zhou, L. Zhang, Adsorption behavior of Pd(II) ions from aqueous solution onto pyromellitic acid modified-UiO-66-NH2. Arab. J. Chem. **13**, 7007–7019 (2020). https://doi.org/10.1016/j.arabjc.2020.07.007
45. R. Ahmad, A. Mirza, Adsorptive removal of heavy metals and anionic dye from aqueous solution using novel xanthan gum-glutathione/zeolite bionanocomposite, Groundwater for. Sustain. Dev. **7**, 305–312 (2018). https://doi.org/10.1016/j.gsd.2018.07.002
46. F. Liu, S. Hua, L. Zhou, B. Hu, Development and characterization of chitosan functionalized dialdehyde viscose fiber for adsorption of Au(III) and Pd(II). Int. J. Biol. Macromol. **173**, 457–466 (2021). https://doi.org/10.1016/j.ijbiomac.2021.01.145
47. J. Zhao, C. Wang, S. Wang, Y. Zhou, B. Zhang, Experimental and DFT studies on the selective adsorption of Pd(II) from wastewater by pyromellitic-functionalized poly(glycidyl methacrylate) microsphere. J. Mol. Liq. **300**, 112296 (2020). https://doi.org/10.1016/j.molliq.2019.112296
48. C. Yan, Z. Cheng, Y. Tian, F. Qiu, H. Chang, S. Li, Y. Cai, X. Quan, Adsorption of Ni(II) on detoxified chromite ore processing residue using citrus peel as reductive mediator: adsorbent preparation, kinetics, isotherm, and thermodynamics analysis. J. Clean. Prod. **315**, 128209 (2021). https://doi.org/10.1016/j.jclepro.2021.128209
49. O. Ayodele, S.J. Olusegun, O.O. Oluwasina, E.A. Okoronkwo, E.O. Olanipekun, N.D.S. Mohallem, W.G. Guimarães, B.L.F. de M. Gomes, G. de O. Souza, H.A. Duarte, Experimental and theoretical studies of the adsorption of Cu and Ni ions from wastewater by hydroxyapatite derived from eggshells. Environ. Nanotechnol. Monit. Manag. **15**, 100439 (2021). https://doi.org/10.1016/j.enmm.2021.100439
50. L. Tang, S. Gou, Y. He, L. Liu, S. Fang, W. Duan, T. Liu, An efficient chitosan-based adsorption material containing phosphoric acid and amidoxime groups for the enrichment of Cu(II) and Ni(II) from water. J. Mol. Liq. **331**, 115815 (2021). https://doi.org/10.1016/j.molliq.2021.115815
51. M. Touihri, F. Guesmi, C. Hannachi, B. Hamrouni, L. Sellaoui, M. Badawi, J. Poch, N. Fiol, Single and simultaneous adsorption of Cr(VI) and Cu (II) on a novel Fe_3O_4/pine cones gel beads nanocomposite: experiments, characterization and isotherms modeling. Chem. Eng. J. **416**, 129101 (2021). https://doi.org/10.1016/j.cej.2021.129101
52. X. Du, S. Cui, X. Fang, Q. Wang, G. Liu, Adsorption of Cd(II), Cu(II), and Zn(II) by granules prepared using sludge from a drinking water purification plant. J. Environ. Chem. Eng. **8**, 104530 (2020). https://doi.org/10.1016/j.jece.2020.104530